Available online at www.sciencedirect.com
SCIENCE DIRECT
Journal of Sound and Vibration 295 (2006) 94–113
JOURNAL OF SOUND AND VIBRATION
www.elsevier.com/locate/jsvi

Wake generator control of inlet flow to cancel flow distortion noise

V. Kota, M.C.M. Wright*

Institute of Sound and Vibration Research, University of Southampton, Southampton SO17 1BJ, UK

Received 16 March 2005; received in revised form 2 December 2005; accepted 19 December 2005
Available online 3 April 2006

Abstract

If the inlet flow to a fan is non-uniform, as is often the case for aircraft engines, then undesirable tonal noise can be generated. A number of authors have suggested using active cancellation to reduce the noise. The secondary field can either be generated by loudspeakers or by the fan itself if secondary non-uniformities are deliberately introduced into the flow. In the research reported here rods inserted radially into the duct were used to generate the secondary field. The distance by which each rod protrudes into the duct was adaptively adjusted in response to an array of in-duct microphones so as to minimise the radiated sound power, whereas previously only fixed rods have been considered. The ability of the steepest-descent algorithm to minimise in-duct sound power under suitable conditions, and hence reduce radiated sound power is demonstrated in both simulations and low Mach number experiments. It is shown how the ability of such a system to control noise depends on the number and position of the controller rods, and the number of acoustic duct modes to be controlled. Thus at low fan speed, when only one mode was present just two controllers achieved an in-duct noise reduction of 25 dB at the blade passing frequency, whereas at a higher fan speed with three modes present six controllers only achieved 2 dB. To implement such a scheme in practice, where large numbers of modes are typically present, it would be necessary to develop controller arrays with many actuators, but with low aerodynamic penalty. Such a system might also be useful in HVAC applications, or in wind-tunnel testing.

1. Introduction

The predicted increased demand on the operation of aircraft in existing airports or creation of new airports increases the scope for noise pollution. Hence, the regulations for new aircraft and engine certification are likely to become more stringent. This is driving the need to explore new methods to control noise. An important component of aircraft engine noise is tonal noise generated by the interaction of fan blades and flow disturbances. The same mechanism can also be a significant factor in other applications, such as HVAC installations and wind tunnels. Tyler and Sofrin [1] explain the interaction mechanism whereby each tone comprises spinning acoustic disturbances whose spatial harmonic order is related to the harmonic order of the flow disturbance. These spinning acoustic disturbances can propagate un-attenuated through the duct only if

*Corresponding author. Tel.: +44 23 8059 2291; fax: +44 23 8059 3190.
E-mail address: mcmw@isvr.soton.ac.uk (M.C.M. Wright).

0022-460X/$ - see front matter © 2006 Elsevier Ltd. All rights reserved.
doi:10.1016/j.jsv.2005.12.050

Nomenclature

a	duct radius
A_{mn}	amplitude of forward propagating mode
B	number of blades
B_{mn}	amplitude of backward propagating mode
c	blade chord
c_0	sound speed in air
$C_{mn,p}$	mode specific coupling coefficient
d	diameter of the control rod
$\hat{D}_{mn,p}$	drag component
i	iteration number
J_m	Bessel function of order m
J	optimisation cost function
k	acoustic wavenumber ω/c_0
l	length of rod
$\mathbf{l}$	control vector of rod lengths
m	azimuthal mode order
M	Mach number
n	radial mode order
N_{mn}	normalization factor for Bessel functions
p	acoustic pressure
P_{sB}	power in harmonic sB
q	number of rod in the controller array
r	radial coordinate
R	reflection coefficient
s	integer multiple
S_c	sears function
$\hat{T}_{mn,p}$	thrust component
U	flow velocity
w	flow disturbance distribution
W	amplitude of flow Fourier–Bessel harmonic
$\mathbf{x}$	position vector
z	axial coordinate
$\alpha_{mn,sB}$	modal wavenumber normalised by free-space wavenumber
β	Mach number parameter $\sqrt{1-M^2}$
$\gamma_{mn,sB}$	quantity defined in Eq. (6)
$\varepsilon_{mn,sB}$	mode constant
ζ	angle of attack
$\eta_{mn,sB}$	mode specific phase of reflection coefficient
θ	azimuthal coordinate
κ_{mn}	nth zero of first derivative of Bessel function of order m
μ	steepest-descent convergence coefficient
$\xi_{mn,sB}$	real part of reflection coefficient
$\pi_{mn,sB}$	modal admittance
ρ_0	density of air
σ_p	reduced frequency
$\phi_{mn,sB}$	imaginary part of reflection coefficient
χ	blade stagger angle
Ψ_{mn}	duct mode shape function
Ω	angular frequency of rotational fan

Subscripts

mn	mode configuration (azimuthal order, radial order)
p	azimuthal mode number of aerodynamic disturbance
sB	blade multiple (usually of the harmonic)
err	error field
pri	primary field
sec	secondary field

Superscripts

D	drag component
H	hermitian transpose
T	thrust component
(q)	rod number
$+/-$	downstream/upstream locations along the duct
0	reference location in the duct (at the fan)
$*$	complex conjugate

they satisfy the duct's cut-on condition, which is that the axial wavenumber should be real, in which case the mode will propagate. If it is not it will be attenuated, and this attenuation will be severe unless the mode is very close to being cut-on, and the tones therefore contain a finite number of modes. The amplitudes of these modes can be related to the amplitudes of the harmonics of the periodic flow disturbance via a model for the blade unsteady forces described by Goldstein [2].

Control of fan noise has been surveyed by Envia [3]. Noise control can be categorized into active and passive techniques. Under passive control, absorbent acoustic liners are laid along several locations of the engine and these provide an impedance boundary condition to the waves reflecting from the walls and attenuate them. The control of noise through treatment is understood to be effective for high-frequency noise as the distance of propagation over the acoustic lining is several wavelengths. Consequently low-speed

machines, which generate relatively low frequencies of noise compared to high-speed machines, require longer lengths of ducting. Modern designs of engines tend to have higher bypass ratios with the result that they require shorter nacelles and hence less length available for treatment.

In active control, noise is controlled by including secondary noise sources in the system, which are driven either in an open or closed loop to produce a secondary field that either cancels or reduces the modes in the primary noise field. In Ref. [3] it was noted that there have been significant noise reduction benefits from the use of active noise control, but that the benefits tend to diminish with the increasing number of simultaneously controlled modes. It was suggested there that this may be due to the multiple modes having a unique phase relationship with each other, and that errors in the measurement of the phase relationship can cause the actuation of the secondary noise sources to produce a noise field that may not exactly match the target field. Furthermore, the power requirements for these secondary noise sources can be high and this has precluded a cost-effective usage or implementation in real engines so far.

The above means of controlling noise represent techniques to control noise at the propagation level in that the sound field is controlled during the propagation process. Attempts to control noise at the source by employing larger rotor–stator spacing and choosing the number of vanes so as to avoid cut-on modes with real axial wavenumber have also been undertaken [4], however a concern with increase in rotor–stator spacing is that it increases the size and hence the weight of the engine. The benefit from the increased spacing is that it reduces the amplitudes of the wakes and hence the intensities of the modes produced through interaction. The cut-off vane count causes the modes generated through interaction to be of a higher order such that they remain cut-on only for the higher harmonics.

Provision of a swept and leaned stator has been proposed as a noise control strategy [5,6]. Sweep is the axial distance and lean is the circumferential displacement of the vane leading edge from its nominal position. By providing sweep and lean on the stator blades 3 EPNdB noise reduction was shown to be possible compared to the situation when a radial stator in its nominal position was used. By providing sweep and lean the contribution to the phase of any mode of the interacting disturbance varies with the span and hence lower levels of noise result from such a design of the stator blading. The limitation of this approach seems to be that it generated more aerodynamic losses than had been anticipated.

Trailing edge blowing has been investigated [7,8]. Flow is supplied through the shaft along a labyrinth of internal passages that start from blade root and terminate at a series of trailing edge ports. Thus the wakes issuing out from the rotor blades are made more uniform so as to cause less unsteady forces on the stator. A test conducted at the NASA Active Noise Control Fan facility [8] demonstrated that the far-field tone power levels in the first three harmonics were reduced by 5.4, 10.6 and 12.4 dB PWL. A blowing rate of 1.6–1.8% (defined as the ratio of the mass flow rate supplied to the trailing edge to the total fan mass flow rate) was found to be optimal.

Another proposal is the provision of a scarfed inlet on the intake to redirect the noise upward. The scarfed inlet is also thought to cause the production of flow distortions which when ingested could produce noise [9].

The effect of boundary layer suction on fan noise was experimentally investigated by Moore [10]. He used a ventilation fan of 1 m diameter with suction applied around the circumference of the duct close to the fan inlet. Upon removal of 5% of the main flow a reduction of 5 dB in the far-field sound power and 15 dB in some of the far-field tones was observed. Progressive reduction in the noise was obtained by proportionately varying the amount of flow bled through suction. He mentions that care must be taken in the design of the bleed system so as not to produce any cut-on residual distortions that could propagate to increase the far-field noise.

Ganz et al. [11] offered new insights into broadband noise mechanisms. They focused their study on broadband noise sources by treating them separately as inflow and self-noise mechanisms. They used a model scale fan rig with provision to bleed the inlet boundary layer and to vary the tip gap and the loading. Self-noise was parametrically studied by varying the tip gap and loading to observe the variation in broadband noise generated through the tip clearance and rotor exit wake flows. The inflow mechanism in this case was isolated by completely removing the inlet boundary layer. To study the inflow noise the boundary layer was re-introduced and its effect was studied on the rotor and stator. Of particular interest is the observation that there was a reduction in the broadband noise through boundary layer suction. They were able to qualitatively explain their results by conducting hot-wire measurements of mean flow velocities and turbulent intensities at the rotor exit.

The field of fluid flow control for the purposes of noise control has been reviewed by Ffowcs Williams [12]. A number of successful schemes have been reported; Sawyer and Fleeter [13] reported a 10 dB reduction in the rotor–stator interaction tones using active airfoil sources mounted on the stator blades. The active airfoil sources were perforated metal covered cavities in the stators that formed resonators and these were driven by compression drivers.

Using a control grid of wake generators Polacsek [14,15] was able to reduce rotor–stator interaction modes with the grid mounted upstream of the rotor. An 8 dB reduction in the SPL at the blade passing frequency (BPF) was achieved by using such a system on the ONERA CERF-rig. Using a CFD–CAA approach to simulate the control he has been able to assess the experimental results. His work was a sequel to an attempt by researchers at ONERA to directly cancel the axial flow velocity defect in a ducted rotor [16].

As mentioned already, methods to alter flow non-unformities seem to have an effect in reducing the unsteady forces on the blades, which consequently reduces the radiated noise. The trailing edge blowing technique, boundary layer removal and the introduction of rods to generate disturbances fall in this category. Nelson [17] theoretically predicted that the tones generated through inlet flow distortions could be used to control a single tone and that optimisation could be done to minimise the total generated sound at higher harmonics of the BPF. His prediction follows from an analytical model due to Goldstein [2], which relates the acoustic response of the fan blades to the intensity of the interacting distorted flow field. Nelson [17] suggested that distortions could be either introduced as positive or negative defects in the velocity profile of a flow field.

A novel way to control this noise is to generate further disturbances that interact with the fan to produce anti-noise. Flow disturbances can be created using an array of cylindrical rods protruding into the duct. The variation of the lengths and orientation of these rods results in the production of wakes of varying extent, which then interact with the fan blades to produce unsteady blade forces and these radiate noise. This actuation method has been previously investigated [15], the work reported here involves the implementation of an adaptive control procedure, whereby an unknown flow distortion is 'tuned out' by an automatic system, which uses in-duct microphones to monitor its effectiveness, in order to minimise far-field radiation. Such a system would have the ability to respond to changing flight conditions.

Such a method would also have a number of disadvantages. The introduction of any wake generator would have a negative effect on aerodynamic performance, which would have to be balanced against any benefits in noise reduction, and benefit would depend upon the application. This balance has not been assessed for the system implemented here because it has not been optimised for aerodynamic impact, which would have to be done before practical application. Furthermore, the addition of such a system to an aircraft engine would increase weight and complexity. If the primary flow disturbance is due to a fixed feature, such as inlet instrumentation or non-circular inlet geometry, then it might be preferable to implement the adaptive system on a prototype engine for a test flight, and to record the converged actuator positions for a series of typical flight conditions. Subsequent production engines could then be fitted with a simpler system that reproduced those actuator positions without the need for the sensing and feedback components of the system.

The goal of this research was to demonstrate experimentally the working of such a control system, albeit at considerably reduced speed and frequency, and to provide insight into the conditions when it might provide a significant acoustic benefit. In order to do so the following research programme was followed. A theoretical model was developed to predict the acoustic response of a ducted fan to an arbitrary frozen flow disturbance, and the particular flow disturbance introduced by a control rod was modelled (Section 2). In this way a cost function based on in-duct sound power could be calculated for any particular setting of an array of control rods. This model was used, in Section 3, to find typical error surfaces (or hypersurfaces), which allowed the investigation of the suitability of the steepest-descent algorithm as a means for adaptively solving this problem, and the optimal placement and arrangement of controllers, which depends on the modal population of the duct. Although the control-space of such a system is typically large and high dimensional the symmetry of the fan and the rod-array was used to reduce this control space. The control procedure having been successfully simulated, control experiments were carried out on a ducted fan (Section 4). The results, given in Section 5 indicate that with sufficient controllers significant noise reduction at the BPF and such harmonics as are included in the cost function is possible, but that if insufficient controllers are available the improvement is greatly limited. These results are discussed in Section 6.

2. Theoretical model

In this section a theoretical model is developed to predict the sound field produced in a semi-infinite duct by an arbitrary frozen (i.e. steady, non-rotating) velocity profile impinging on a steadily rotating fan. The aeroacoustic treatment is based on that of Goldstein [2] and adheres to the same notation as far as is practicable. This model is used to formulate the response to an array of wake generators, whose influence on the base flow is assumed to add linearly and also to linearly superimpose on the primary flow distortion. By using in-duct sound power as a cost function an optimisation problem is defined, which can be adaptively solved by use of the steepest-descent algorithm.

2.1. Acoustics of ducts with uniform flow

The coordinate system (r, θ, z) for the fan duct with incident and reflected modes is shown in Fig. 1. The pressure in any harmonic, p_{sB}, where B is the number of blades in the fan, evaluated at a defined location $\mathbf{x}$ within the duct is expressed as a sum of weighted cut-on modes. The equation for pressure at any upstream or downstream location along the duct is

$$p_{sB}(\mathbf{x}) = \sum_{p=-\infty}^{+\infty} \sum_{n=1}^{+\infty} \left(A_{mn}^{\pm} \mathrm{e}^{-\mathrm{j}k_{mn}^{z+}z} + B_{mn}^{\pm} \mathrm{e}^{-\mathrm{j}k_{mn}^{z-}z} \right) \Psi_{mn}(r, \theta), \tag{1}$$

where A_{mn} and B_{mn} represent the amplitudes of the forward propagating and backward propagating mode systems, the $+/-$ superscripts on A_{mn} and B_{mn} refer to regions downstream/upstream of the fan. The duct mode shape function is represented by $\Psi_{mn}(r, \theta) = (\mathrm{J}_m(\kappa_{mn} r)/N_{mn})\, \mathrm{e}^{-\mathrm{j}m\theta}$ with m and n being their circumferential and radial orders, and $N_{mn}^2 = \int_S \mathrm{J}_m^2(\kappa_{mn} r)\, \mathrm{d}S$ is the usual shape function normalisation factor. The axial wavenumber is $k_{mn}^{z\pm} = \pm(\sqrt{k_0^2 - \beta^2 \kappa_{mn}^2} - Mk_0)/\beta^2$, which is related to the free space wavenumber k_0 and M, the flow Mach number. The $+/-$ superscripts on the axial wavenumber k_{mn}^z refer to those of either the backward or forward propagating mode. The modal amplitudes $A_{mn}^{\pm}$ and $B_{mn}^{\pm}$ are related through the reflection coefficients $R_{mn}^{\pm}$ as described by Morfey [18] so that

$$\begin{aligned} R_{mn}^{+} &= \frac{B_{mn}^{+}}{A_{mn}^{+}} = \mathrm{e}^{2\mathrm{j}\eta_{mn}^{0+}}, \\ \frac{1}{R_{mn}^{-}} &= \frac{B_{mn}^{-}}{A_{mn}^{-}} = \mathrm{e}^{2\mathrm{j}\eta_{mn}^{0-}}, \end{aligned} \tag{2}$$

where $\eta_{mn}^{0\pm}$ is the complex reflection phase at the downstream/upstream duct ends. Restricting our attention to the upstream side of the fan in order to control the noise on the inlet side, pressure can be expressed in terms of the upstream backward propagating modal amplitude B_{mn}^{-}:

$$p_{sB}^{-}(x) = \sum_{p=-\infty}^{+\infty} \sum_{n=1}^{+\infty} 2B_{mn}^{-} \mathrm{e}^{\mathrm{j}[-\eta_{mn}^{0-} + (MsB\Omega/c_0\beta^2)z]} \cos\left[\eta_{mn,sB}^{-}(z)\right] \Psi_{mn}(r, \theta), \tag{3}$$

where $\eta_{mn,sB}^{-}(z)$ is the complex reflection phase that varies along the axis and is given by

$$\eta_{mn}^{\pm}(z) = \eta_{mn}^{0\pm} + \frac{k_{mn}}{\beta^2} z, \quad k_{mn} = \sqrt{k_0^2 - \beta^2 \kappa_{mn}^2}. \tag{4}$$

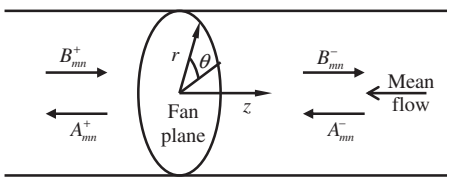

Fig. 1. Coordinate system in the fan duct with incident and reflected modes.

A mode of circumferential order m is excited by a flow disturbance of harmonic order p, the relationship between them being given by the Tyler–Sofrin formula $m = sB-p$, where B is the number of blades and s is an integer.

2.2. Sound generation

The modal amplitudes are obtained from the theoretical model of Goldstein [2], which assumes that the fan blades can be treated as flat plates at a small angle of attack (thus simplifying the form of their contribution to the Ffowcs Williams–Hawkings equation) whose fluctuating forces act as dipole sources in an infinite duct. Pitelet [19] extended this model to the case of a finite duct to take the end reflections into account. This was extended for a semi-infinite duct approximation to account for the case where there is an anechoic termination at the outlet [20]. The resulting expression for pressure is

$$\begin{aligned} p^-_{sB}(x) &= B\sum_{p=-\infty}^{\infty}\sum_{n=1}^{\infty}\frac{\mathrm{J}_m(\kappa_{mn}r)\mathrm{e}^{-\mathrm{j}m\theta}}{N^2_{mn}k_{mn,sB}}\mathrm{e}^{-\mathrm{j}\eta^{0-}_{mn}}(m\hat{D}_{mn,p}+\gamma^-_{mn,sB}\hat{T}_{mn,p})\ \exp\left(\mathrm{j}\frac{MsB\Omega}{c_0\beta^2}z\right)\ \cos\left(\eta^-_{mn,sB}(z)\right)\\ &= \frac{B}{2}\sum_{p=-\infty}^{\infty}\sum_{n=1}^{\infty}\frac{\mathrm{J}_m(\kappa_{mn}r)\mathrm{e}^{-\mathrm{j}m\theta}}{N^2_{mn}k_{mn,sB}}\mathrm{e}^{-\mathrm{j}\eta^{0-}_{mn}}(m\hat{D}_{mn,p}+\gamma^-_{mn,sB}\hat{T}_{mn,p})\\ &\quad\times\left[\exp\ \mathrm{j}\left(\frac{MsB\Omega}{c_0\beta^2}z+\eta^-_{mn,sB}(z)\right)+\exp\ \mathrm{j}\left(\frac{MsB\Omega}{c_0\beta^2}z-\eta^-_{mn,sB}(z)\right)\right], \end{aligned} \tag{5}$$

where

$$\gamma^-_{mn,sB} = -\frac{k_{mn,sB}}{\beta^2}-\frac{MsB\Omega}{c_0\beta^2}, \tag{6}$$

and $\hat{D}_{mn,p}$ and $\hat{T}_{mn,p}$ are the unsteady blade drag and thrust forces

$$\begin{aligned} \hat{D}_{mn,p} &\equiv -\frac{c}{2}\rho_0 U_r\ \cos\ \chi\ \sin\ \zeta\ S_c(\sigma_p,M_r)W^D_{mn,p},\\ \hat{T}_{mn,p} &\equiv -\frac{c}{2}\rho_0 U_r\ \sin\ \chi\ \sin\ \zeta\ S_c(\sigma_p,M_r)W^T_{mn,p}, \end{aligned} \tag{7}$$

where S_c is the Sears function for a compressible flow, χ and ζ are the fan blade's angles of stagger and attack, $\sigma_p = p\Omega c/2U_r$ is the reduced frequency and W^T and W^D are the Fourier–Bessel flow distortion harmonics, which are obtained from the flow disturbance by

$$\begin{aligned} W^D_{mn,p} &= \int_0^a\int_0^{2\pi}\mathrm{e}^{-\mathrm{j}p\theta_s}\mathrm{J}_m(\kappa_{mn}r_s)\ w(r_s,\theta_s)\frac{1}{r_s}\ \mathrm{d}\theta_s\ \mathrm{d}r,\\ W^T_{mn,p} &= \int_0^a\int_0^{2\pi}\mathrm{e}^{-\mathrm{j}p\theta_s}\mathrm{J}_m(\kappa_{mn}r_s)\ w(r_s,\theta_s)\ \mathrm{d}\theta_s\ \mathrm{d}r_s. \end{aligned} \tag{8}$$

The quantity, $(m\hat{D}_{mn,p}+\gamma^-_{mn,sB}\hat{T}_{mn,p})$, shall henceforth be called the coupling coefficient, $C_{mn,p}$.

2.3. Cost function

Assuming that the interaction between multiple controllers is linear, the total acoustic field resulting from the presence of the controllers can be considered as a superposition of the primary field from the primary flow disturbance $w_{\mathrm{pri}}(r,\theta)$ and the secondary field from the secondary flow disturbance $w_{\mathrm{sec}}(r,\theta)$. The coupling coefficient for the total or error field is

$$C_{\mathrm{err}} = C_{\mathrm{pri}} + C_{\mathrm{sec}} \tag{9}$$

The power in a single harmonic is obtained from the expression given by Morfey [18], which takes into account the reflections through modal admittances defined as $\pi_{sB,m,n} = \rho_o c_o p_{sB,m,n}/u_{sB,m,n}$, where $p_{sB,m,n}$ is the pressure and $u_{sB,m,n}$ is the axial acoustic velocity. The expression for sound intensity given in Ref. [18] is dependent on $\pi_{sB,m,n}$, which is a function of the complex reflection phase $\eta_{sB,m,n}$, with real and imaginary parts

$\xi_{sB,m,n}$ and $\phi_{sB,m,n}$, respectively. The expression for power obtained by integrating the intensity over the duct cross section depends only on the imaginary part $\phi_{sB,m,n}$ of the reflection phase:

$$P_{sB}^{-} = \frac{B^2}{2\rho_0 c_0} \sum_{p=-\infty}^{\infty} \sum_{n=1}^{\infty} \frac{1}{N_{mn}^2 k_{mn,sB}^2} \frac{\alpha_{mn,sB}\beta^4}{(1-\alpha_{mn,sB}^2 M^2)^2} e^{2\phi_{mn,sB}^{0-}} \times \left[-e^{2\phi_{mn,sB}^{0-}} (1+\alpha_{mn,sB}M)^2 + e^{-2\phi_{mn,sB}^{0-}} (1-\alpha_{mn,sB}M)^2 \right] \left| m\hat{D}_{mn,p} + \gamma_{mn,sB}^{-} \hat{T}_{mn,p} \right|^2, \tag{10}$$

where $\alpha_{mn,sB} = k_{mn,sB}/k_0$.

Excepting the term for the coupling coefficient, which is dependent on the control vector, the rest of the terms in this expression can be considered a constant specific to each mode, so power P_{sB} can be written as

$$P_{sB} = \sum_{p=-\infty}^{\infty} \sum_{n=1}^{\infty} \varepsilon_{mn,sB} \left| C_{mn,p} \right|^2. \tag{11}$$

2.4. Optimisation algorithm

The cost function J is a summation of the powers in the number of harmonics chosen for optimisation

$$\begin{aligned} J &= \sum_{sB} P_{sB} = \sum_{sB} \sum_{mn,p} \left(C_{\text{err}}^{*} C_{\text{err}} \right) \varepsilon_{mn,sB} \\ &= \sum_{sB} \sum_{mn,p} \left(C_{\text{pri}} + C_{\text{sec}} \right)^{*} \left(C_{\text{pri}} + C_{\text{sec}} \right) \varepsilon_{mn,sB}. \end{aligned} \tag{12}$$

If required this could be replaced by a weighted sum without difficulty. The net coupling coefficient for the secondary field can be considered as a linear superposition of the coupling coefficients associated with each control rod

$$C_{\text{sec}} = \sum_{q} C_{mn,p}^{(q)}. \tag{13}$$

Each of these $C_{mn,p}^{(q)}$ will be a function, not necessarily linear, of the length of the corresponding rod length, l_q. If this nonlinearity is sufficiently mild then the dependence of J upon $\mathbf{l}$, the vector of rod lengths, will have a global minimum.

The steepest-descent algorithm [21] (also known as the gradient descent algorithm) is an attractive candidate for this optimisation, due to its simplicity and robustness. Determination of the optimum control vector by this method requires its iteration along the steepest-descent of the cost function

$$\mathbf{l}(i) = \mathbf{l}(i-1) - \mu \frac{\partial J}{\partial \mathbf{l}} \tag{14}$$

where μ is a convergence coefficient that determines the rate of convergence. Its optimum value depends on the shape of the error surface, in practice a smaller value is usually chosen by trial and error to ensure a stable convergence. Differentiating Eq. (12) with respect to $\mathbf{l}$ and observing that the primary coupling coefficient is a constant the following expression is obtained for the control vector derivative of the cost function.

$$\frac{\partial J}{\partial \mathbf{l}} = \sum_{sB} \sum_{mn,p} 2\text{Re} \left[\left(\frac{\partial C_{\text{sec}}}{\partial \mathbf{l}} \right)^{H} C_{\text{err}} \right] \varepsilon_{mn,sB}. \tag{15}$$

The control vector derivative of the cost function $\partial J/\partial \mathbf{l}$ is thus expressed in terms of the secondary field coupling coefficient $\partial C_{\text{sec}}/\partial \mathbf{l}$.

2.5. Rod wake model

In order to simulate the control procedure it is necessary to model the flow disturbance generated by the insertion of a control rod into the duct. In order to calculate the modal coupling coefficients of the controller

rods a wake model for the wake profile $w_q(r,\theta)$ generated by each control rod q, as given by Polacsek [14], is assumed. This model assigns a normal distribution along the circumferential coordinate θ for the velocity distribution of a wake, w_q, generated by an infinitely long rod and was extended by Pitelet [19] to account for the end effect of a finite rod of length l_q and diameter d located at (θ_q, z_q) within the duct to give

$$w_q(r,\theta) = U\sqrt{\frac{d}{z_r}}\exp\left[-\frac{\pi}{z_q d}\left(\frac{r(\theta-\theta_q)}{0.8}\right)^2\right]\exp\left[-\frac{\pi}{z_q d}\left(\frac{a-l_q-r}{0.8}\right)^2\right] \tag{16}$$

Of course, unsteady vortex shedding will also be expected when a cylinder is placed in a mean flow, but computational modelling suggests that this will be outweighed by the contribution from the steady part of the velocity defect [14]. Eq. (16) can be substituted into the expressions in Eq. (8) to obtain the Fourier–Bessel decomposition of the wake profile so as to estimate the thrust and drag coefficients and hence the modal coupling coefficients.

2.6. Conditions for controllability

Consider the case where there are three modes to be controlled, with azimuthal mode orders $m = -1, 0, 1$ (radial mode order $n = 1$ throughout) and 8 equally spaced controllers are available to control these modes (as, in fact, is the case with the fan rig described later). For simplicity let the modal phase for the reference controller in each case be 0°. The phase contribution to the $m = 1$ mode from the 8 rods is then

$$e^{-jp\theta} = e^{-j(8\times q\times 2\pi/8)} = 1 \quad \text{for} \quad q = 0,\ldots,7, \tag{17}$$

based on the Tyler–Sofrin formula given above. This expression shows that all rods generate an in-phase contribution for mode $m = 1$ (for which $p = 8$). Similarly the phase contribution to the mode $m = 0$ (for which $p = 9$) from the 8 rods is given by

$$e^{-jp\theta} = e^{-j(9\times q\times 2\pi/8)} \quad \text{for} \quad q = 0,\ldots,7, \tag{18}$$

so half the number of rods generate an out of phase contribution. Substituting other values for q it can be seen that the contribution of rods $q = 0, \ldots, 3$ is opposite in phase to that of rods $q = 4, \ldots, 7$. Likewise the phase contribution to the $m = -1$ mode from the 8 rods is given by

$$e^{-jp\theta} = e^{-j(10\times q\times 2\pi/8)} \quad \text{for} \quad q = 0,\ldots,7, \tag{19}$$

so that half the number of rods generate an out of phase contribution for mode $m = -1$ (for which $p = 10$). Substituting $q = 0, \ldots, 7$ it can be seen that the contribution of rods $q = 0$, 1, 4 and 5 are opposite in phase to that of rods $q = 2$, 3, 6 and 7.

Considering the problem of having to control three modes simultaneously, it is seen that the 8 rods produce an in-phase contribution for mode $m = 1$. If all 8 rods are used to control the three modes, it would require a simple re-orientation of the controller array to make the rod-generated contribution to mode $m = 1$ out of phase with respect to the corresponding primary disturbance mode. Further assume that the 8 rods have equal length, so that each rod makes an equal contribution to the anti-phase mode that is being generated. Having adjusted the orientation of the array to control the mode $m = 1$ the array will now be unable to control the other two modes $m = 0, -1$, because for these two modes half the rods on the array generate an anti-phase contribution to that of the other half. If half the array rods were set to zero lengths, then attempting to control the $m = 1$ mode by adjusting the lengths of the remaining rods would not result in a self-cancelling contribution to the $m = 0$ mode since the modal amplitude vectors on any consecutive half of the 8 rod array lie in a half-plane. Assuming now that modes $m = 1$ and $m = 0$ are controlled by readjusting the lengths of the 4 rods, it is now possible to examine the control of mode $m = -1$ using half of the 8 rods used to control the other two modes. It can be seen that the half of the array that was used to control the other two modes is now arranged so that half of the 4 rods produce an out of phase contribution with respect to the other half for the last mode $m = -1$. It can therefore be seen that as more modes are introduced into the control system, using more controllers becomes less effective. Only a quarter of the controllers on the 8-rod array are effective for controlling the three modes mentioned above.

This analysis indicates that the effectiveness of an equally spaced array of 8 rods will be reduced at fan speeds that are sufficiently high for these three modes to be present.

2.7. Limitations of the model

The model of the rod–fan interaction contains a number of simplifying assumptions. The fan-noise model assumes that the fan blades are flat plates at low incidence, which is often a reasonable assumption for aircraft engines but is less justifiable for ventilation fans such as the one used in the experiments here, so the absolute amplitudes predicted are likely to be inaccurate. The model of the rod wake does not take into account changes in the end effects when the rod length is very short, and also assumes that the mean flow contains no swirl component so that the wake that impinges on the fan is directly behind the rod. The model also assumes that there is no interaction between rod wakes when several rods are present, and that the effect of the rods on the mean flow velocity through the fan is negligible. The validity of these assumptions will be examined when the simulation results are compared with the experiments.

3. Numerical simulation of control of multiple modes with multiple controllers

Before undertaking the experimental evaluation of such a system the situation was simulated using the theoretical model described in the previous section so as to give insight into its likely behaviour. The number of fan blades and controllers for the experimental system were already fixed by circumstances outside the investigators' control, so the simulation also allowed the investigation of the effects of using different numbers of controllers.

3.1. Simulated fan conditions

Simulation of control of fan noise was conducted using a random disturbance in the flow velocity field, generated by assigning Gaussianly distributed random numbers to domains in the fan cross-section obtained by imposing an r, θ mesh over the cross-section such that the smallest element was much smaller than the chord of a fan blade. The physical conditions were chosen to match those of the experimental system. The speed of the fan was 3000 revolutions per minute giving a BPF of 450 Hz; the number of blades on the fan was 9, the tip diameter of the fan was 630 mm and the control rod diameter was 12 mm. The random disturbance excites three cut-on modes at BPF of 450 Hz, namely modes with circumferential order $m = -1, 0, 1$. The defect generates the primary acoustic field, which needs to be controlled, and hence the quantity C_{pri} represents the coupling coefficients of each of the modes present in the primary acoustic field at BPF for the disturbance. The cost function J, taken to be the power in just the first harmonic, is optimised by iteratively proceeding along the steepest gradient of J and obtaining the optimum vector of lengths $\mathbf{l}$ and the optimum residual power.

3.2. Simulation results

In order to investigate the effect of using increased numbers of controllers the number of equally spaced rods used to control the random disturbance was increased from 1 through 20, and the variation of the minimised cost function with the phase of the rod array in each case was determined. The minimum from this phase characteristic was determined and the variation of this minimum is plotted against the number of controllers that were stepped through in Fig. 2. The primary power without control in each harmonic is also shown in the figure so that the reduction in the power in each control case can be inferred by comparing the variation of the minimised cost function with the primary power. It can be seen that the reduction obtained through control decreases as the number of harmonics being controlled increases. Though there is increased reduction as the rods increase to 20, this is not gradual. As already mentioned the variation illustrated in Fig. 2 is that which is obtained after collation of the best minimisations happening at particular orientations of the rod array in each rod array case. These orientations are different for each rod array case. Also these best orientations for each rod array case were examined to see if they have any relationship with the phases of the

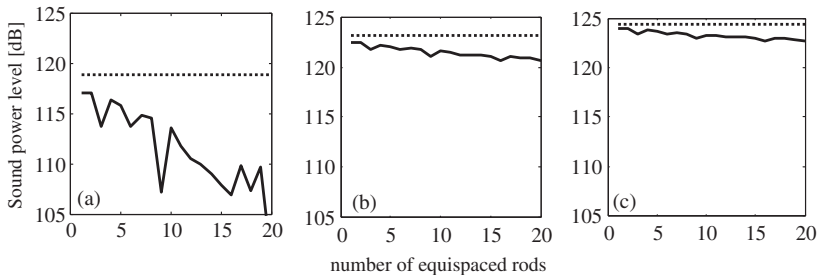

Fig. 2. Simulated variation of minimised noise power against the number of equally spaced controllers for the random primary flow disturbance after attempting to control (a) one, (b) two and (c) three harmonics of BPF. · · · · · primary sound power, ——— residual sound power.

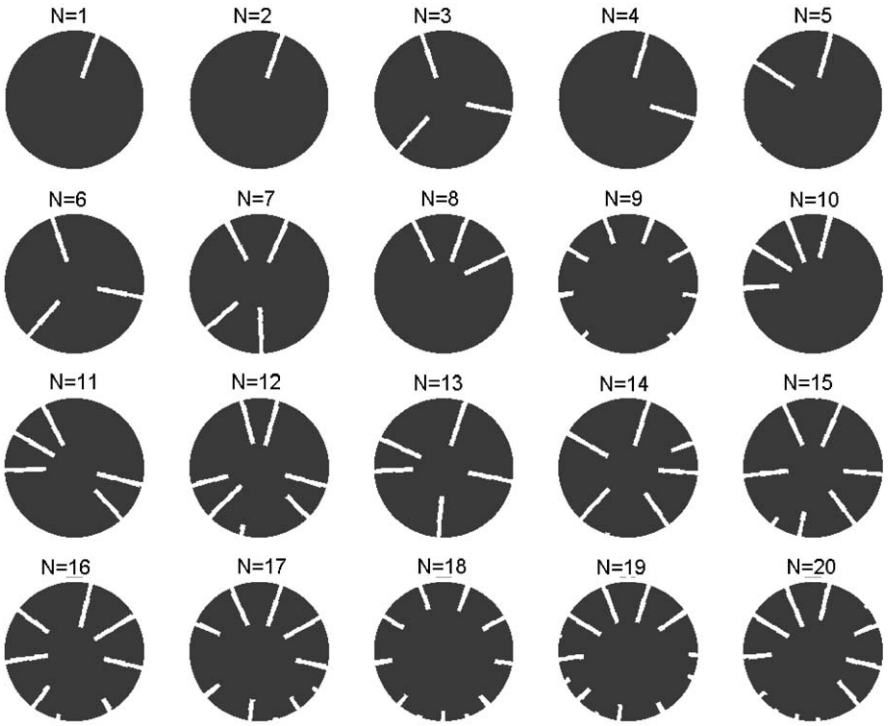

Fig. 3. Simulated configurations of the converged rods in the equally spaced rod cases with the 1st Harmonic optimised (N = number of equally spaced rods used).

three modes in the first harmonic. No such simple relationship was found as was shown to exist in the cancellation of the single mode. These results suggest that it is through running the algorithm that one should determine the positioning of the array in each individual case.

For the best orientations discussed previously in the individual cases of control using 1–20 equally spaced rod cases, the configuration of the converged rod lengths are shown in Fig. 3. Similar such configurations were obtained when the subsequent harmonics were also included in the control cost function.

4. Experimental investigation

4.1. Test facility

A schematic of the fan rig in the anechoic chamber is shown in Fig. 4 and the details of the fan duct in Fig. 5. The chamber was anechoic to frequencies above 300 Hz. The fan rig consisted of a 630 mm duct

housing the 9-bladed fan preceded by an inlet, microphone array rings, a controller rod array ring and followed by an anechoic duct termination manufactured according to BS EN ISO 5136 [22]. The air discharged into a plenum chamber with six vents for recirculation of air into the main chamber. Neither the duct inlet nor the plenum return vents were optimised for aerodynamic performance and the levels of unsteady flow and noise within the lab were higher than desirable. Full technical details are given in Kota [20].

The fan was run at 1767 and 2934 rev/min, hereafter referred to as the low-speed and high-speed cases. An optical triggering device was used to detect the rotation of the fan and synchronise measurements.

The controller rod array is shown in Fig. 6. It consisted of radial rods equally spaced circumferentially on a cylindrical ring. The rods could be made to translate radially and the ring as a whole could be rotated under computer control by the use of stepper motors. These motions were constrained to 200 mm of length and 30° of rotation. The diameter of the rods was 12 mm.

The microphone array consisted of 5 cylindrical rings with circumferentially spaced flush mounted microphones. A maximum of up to 24 microphones could be fixed on each ring. The centres of the five rings had an axial separation of 98 mm.

4.2. Processing

The pressure signals from the microphones were Fourier transformed using vector averaging of FFT estimates over blocks of these signals phase locked with the fan. Each block's length corresponded to a single revolution of the fan and the averaging was performed over 400 blocks at the low speed and 600 blocks at the high speed. These values were chosen after a detailed analysis of the excessive aerodynamic noise of the system (see Ref. [20] for full details). Even with these numbers of averages the signals remained noisy, as can be seen from the results below, but the values chosen reflected a compromise between noise and speed.

Since the cost function for the active control algorithm, i.e., the overall sound power level J, is expressed as the squared sum of the modal amplitudes in the tones of the total noise field, these need to be obtained by decomposing the tones obtained from the FFTs into modes. If only inlet radiated noise is considered for control and attention is restricted to the cut-on modes at the BPF, then the expression for the acoustic pressure at this harmonic is given by Eq. (1) but with finite sums:

$$p_{sB}^{-}(\mathbf{x}) = \sum_{m,n} (A_{mn}^{-} \mathrm{e}^{-\mathrm{j}k_{mn}^{z+}z} + B_{mn}^{-} \mathrm{e}^{-\mathrm{j}k_{mn}^{z-}z}) \Psi_{mn}(r,\theta). \tag{20}$$

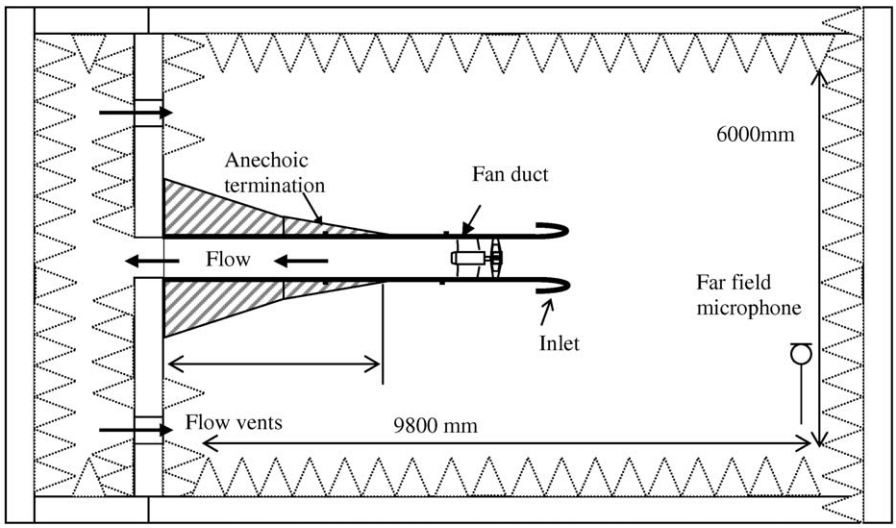

Fig. 4. Schematic of the fan rig.

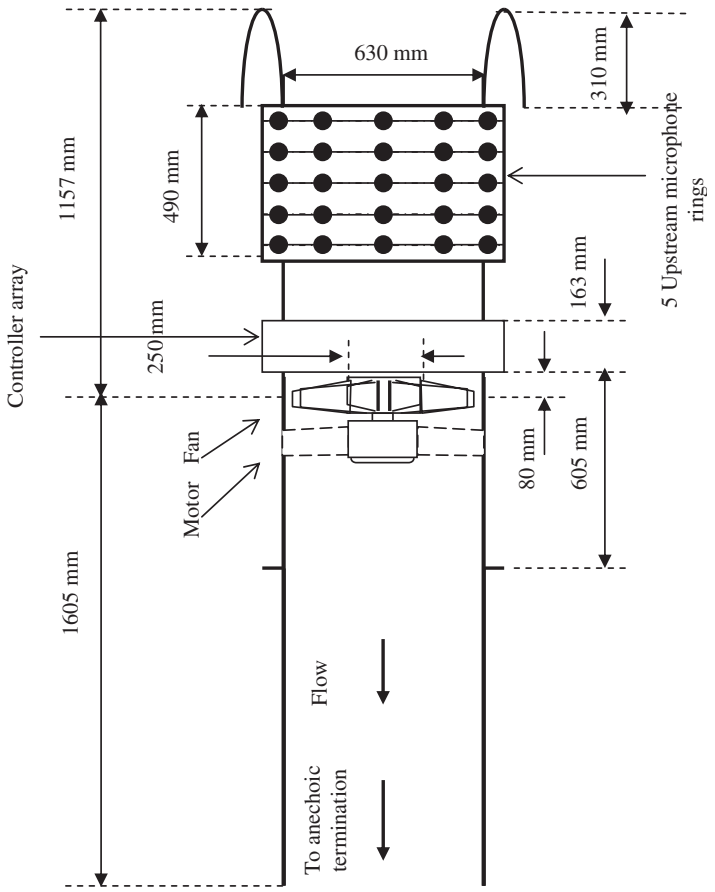

Fig. 5. The fan duct.

When related to the data obtained from the signals of the microphone array this becomes a system of linear equations where the left side is the column vector of the tonal pressures and the right side involves the unknown cut-on modal amplitudes, A^{-}_{mn} and B^{-}_{mn}, and terms that depend on the microphone locations (z, θ).

Referring to Eq. (5) for the acoustic pressure field in terms of the coupling coefficient and expressing this in terms of the upstream incident modal amplitude B^{-}_{mn},

$$p_{sB}(x) = B \sum_{p=-\infty}^{\infty} \sum_{n=1}^{\infty} \frac{\mathrm{J}_m(\kappa_{mn} r) \mathrm{e}^{\mathrm{j}(MsB\Omega/c_0\beta^2)z} \mathrm{e}^{-\mathrm{j}m\theta}}{N^2_{mn} k_{mn,sB}} \mathrm{e}^{-\mathrm{j}\eta^{0-}_{mn}} \cos\left[\eta^{-}_{mn,sB}(z)\right](m\hat{D}_{mn,p} + \gamma^{-}_{mn,sB}\hat{T}_{mn,p})$$

$$= \sum_{p=-\infty}^{\infty} \sum_{n=1}^{\infty} 2B^{-}_{mn} \mathrm{e}^{\mathrm{j}[-\eta^{0-}_{mn} + (MsB\Omega/c_0\beta^2)z]} \cos\left[\eta^{-}_{mn,sB}(z)\right] \Psi_{mn}(r, \theta), \tag{21}$$

the value of the coupling coefficient $C_{mn,p}$ can be extracted as follows:

$$C_{mn,p} = (m\hat{D}_{mn,p} + \gamma^{-}_{mn,sB}\hat{T}_{mn,p}) = \frac{B^{-}_{mn}(2N_{mn}\, k_{mn,sB})}{B} \tag{22}$$

The contribution of the rod to the acoustic field, i.e., C_{sec} can then be calculated from

$$C_{\mathrm{err}} - C_{\mathrm{pri}} = C_{\mathrm{sec}} \tag{23}$$

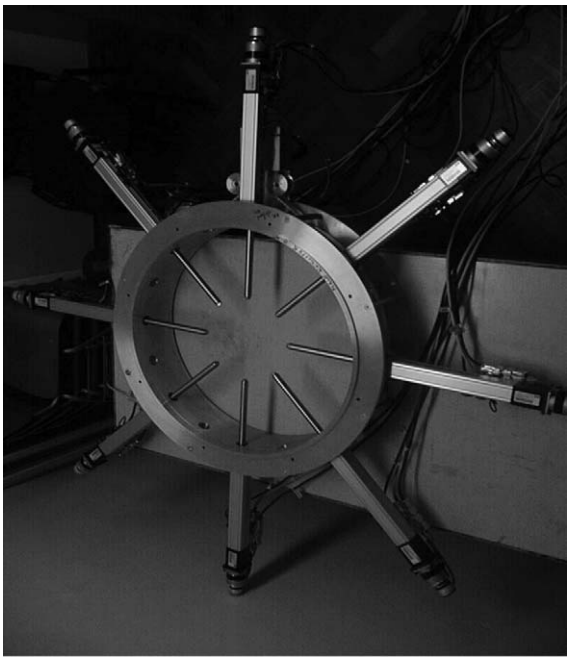

Fig. 6. The 8-rod array.

When using multiple rods or rotating a single rod while implementing the active control system the theoretical response of the multiple rods or the rotated rod is obtained using the relation: $C^{(q)}_{mn,p} = e^{-jp\theta_q} C^{(1)}_{mn,p}$.

5. Results

5.1. Acoustic response

Before attempting the practical implementation of the control system the acoustic response of the rods in terms of the coupling coefficients needs to be experimentally determined. This response can subsequently be used for any control operation. A single cylindrical rod was fixed at the azimuthal zero reference and its length was varied in steps of 10 mm each and the signals from the microphones were captured and processed as described above to obtain the acoustic response in terms of the modal coupling coefficient. The fan was run at the said speeds and the BPFs for these speeds correspond to 262 Hz (low-speed setting) and 441 Hz (high-speed setting). At the BPF for the low speed, only the plane wave mode ($m = 0$) is cut-on. At the BPF for the high speed case 3 modes ($m = -1, 0, 1$) are cut-on in the first harmonic. Only the acoustic response for the first rod in terms of the modal coupling coefficient amplitude and phase for the plane wave mode alone ($m = 0$) are shown in Fig. 7 for the two fan speeds. The responses for the other rods and the other cut-on modes at the high fan speed are similar to those given for the plane wave mode. The phase response is nearly flat but exhibits a drift in the lower length range. This could be due to the fan itself inducing a radially varying swirl in the wake generated by the rod, which would cause the wake to shift circumferentially as it travels towards the fan. It could also be due to end effects of the rod, which would become more significant at short lengths, or because for short rods the secondary field is weak and may be overwhelmed by the background noise. Since the drift is similar for all the rods, and the control algorithm responds to local rather than global inputs the control process will still be effective. The amplitudes can be seen to be steadily rising as expected.

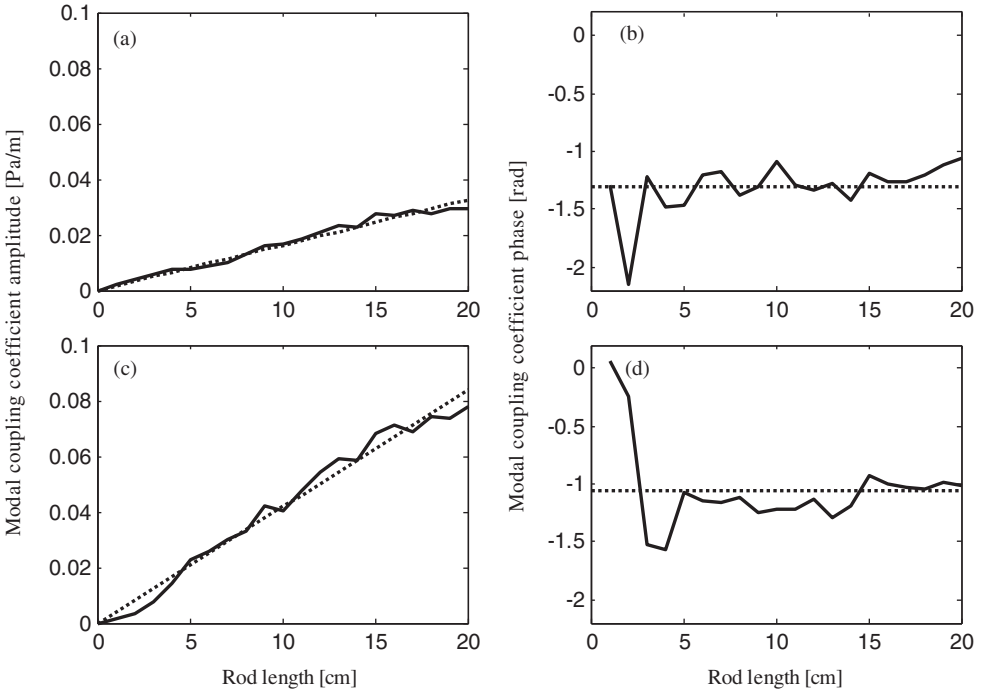

Fig. 7. Measured amplitude ((a) & (c)) and averaged phase ((b) & (d)) of the coupling coefficient of rods on the controller array for the plane wave mode at low ((a) & (b)) and high ((c) & (d)) fan speeds. · · · · · theoretical prediction, ——— measured.

5.2. Active control experiments at low speed

In order to demonstrate the working of the algorithm to control noise using the rod array experiments were performed at the low speed where there was only one mode cut-on. In these experiments a single rod (rod 1 on the array) was used as a source and two other rods (rods 3 and 5 on the array) were used as controllers to demonstrate noise control. Constraints were handled by saturation, that is, whenever the algorithm required a rod length outside the feasible range 0–20 cm the length was held at the limit of the range.

All the control cases involving the control of the plane wave mode at the low speed as mentioned previously were conducted using rod 1 as the source and rods 3 and 5 as the controllers. Rod 1 was fully extended into the duct (20 cm) to excite the primary disturbance mode. The success of the steepest-descent strategy used depends on the shape of the cost function surface induced by the physical problem. Consider the following assumptions that might be made about the influence of the rod lengths upon the coupling coefficients:

(i) The coupling coefficients $C_{mn,p}^{(q)}$ depend linearly upon the rod lengths l_q.
(ii) The rod responses differ only by a constant phase factor such that $C_{mn,p}^{(q)} = \mathrm{e}^{-\mathrm{j}p\theta_q} C_{mn,p}^{(1)}$.
(iii) Each coupling coefficient is independent of all other rod lengths.

If all of these assumptions are satisfied then the induced surface will be quadratic and, if positive definite, have a single unique optimum. In reality these assumptions are likely to be only approximately satisfied. The effect of their departures from the ideal was therefore investigated by obtaining the cost function surface for this two-dimensional control problem with successive assumptions removed. The results are shown in Fig. 8. To produce plot (a) the response of rod 1 was linearised and the responses of the other rods obtained from it so that assumptions (i)–(iii) were satisfied. For (b) the true amplitude response of rod 1 was used and the responses of the other rods were obtained from it so that assumptions (ii) and (iii) were satisfied. For (c) the amplitude and phase response of each rod was measured and the results were linearly combined so that only

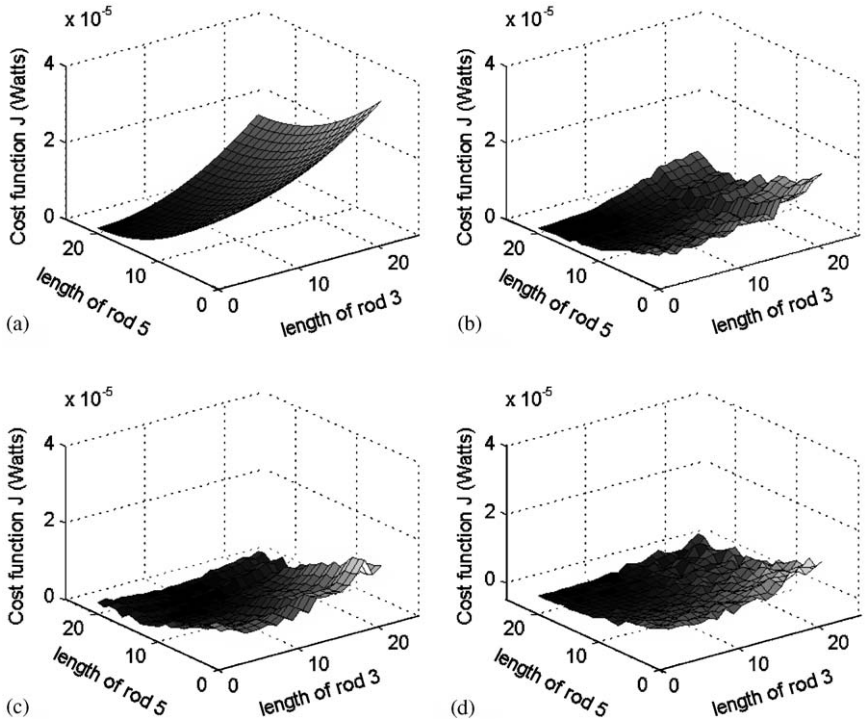

Fig. 8. Simulated and measured cost function surface plots formed by using rod 1 fully extended as the source of the primary flow disturbance and varying the lengths of rods 3 and 5. (a) Surface found by assuming a linear response to each rod, an ideal phase relationship between rods and no interaction between rods. (b) Surface found by using the measured amplitude response to one rod and assuming an ideal phase relations between rods and no interaction between rods. (c) Surface found by using measured amplitude and phase for each rod and assuming no interaction between rods. (d) Actual measured error surface when rods 3 and 5 are set to their individual lengths in the duct.

assumption (iii) was satisfied. Finally, for (d) the cost function was measured directly on the fan rig so that no assumptions needed to be made.

The shape of (a) is somewhat different to the others and has its minimum at the origin, whereas for the others it is slightly displaced. This indicates that assumption (i), namely that the response is linear in rod length is not justified. The similarity of (b)–(d) indicates that assumptions (ii) and (iii) are valid in this case. The effect of the noise can clearly be seen in these figures, and must be taken into account by reducing the convergence coefficient so that local variations in the surface do not lead to sudden departures from the desired trajectory.

The algorithm was then tested for different convergence coefficients and initial conditions (with both control rods set to 0 cm length or one rod set to 0 cm and the other set to 20 cm) and it was found that a choice of the convergence coefficient of $\mu = 2.5 \times 10^6$ led to suitably steady convergence. The results of control are given below. The convergence of lengths and in-duct power level variations are given in Fig. 9. In a few cases the amplitude of the tone was negligible in amplitude compared with the background noise in the duct, and incoherent in its phase across the blade passing segments; this produced a measurement corresponding to mean energy flow toward the fan instead of away from it. The in-duct power reduced from 67 to 52 dB but with considerable variance in the converged value.

Finally, the trajectory of the control algorithm in **l**-space is superimposed on the error surface contour J for two control cases in Fig. 10. The trace of convergence for the fine-tuned convergence coefficient is shown for an example with an initial condition of rod 3 set to 20 cm and rod 5 to 0 cm. With the same convergence coefficient a second example is shown for a different initial condition (with rods 3 and 5 retracted). In each case they converged to approximately the same minimum.

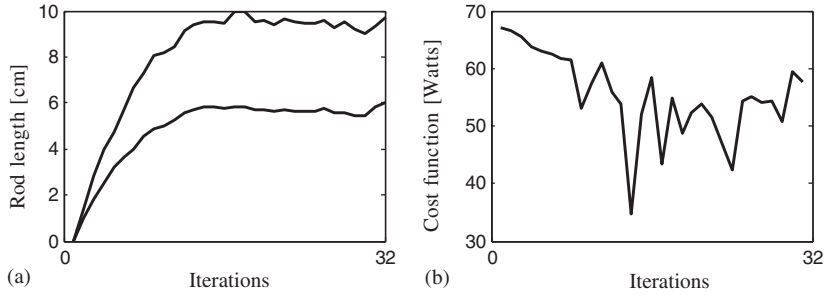

Fig. 9. (a) Measured length and (b) cost function convergences for control experiment with two control rods at low fan speed. The convergence coefficient $\mu = 2.5 \times 10^6$, with an initial condition of controller rods 3 and 6 fully retracted.

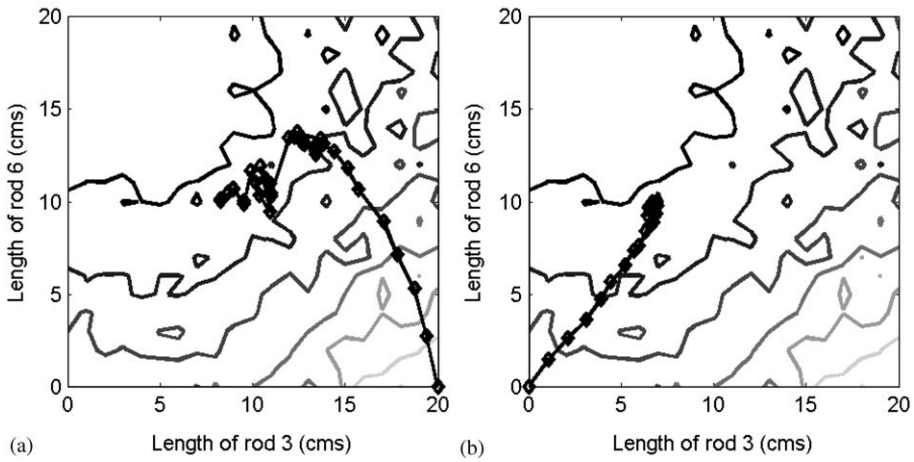

Fig. 10. Measured control trajectory superimposed on the measured cost function contours at low speed with $\mu = 2.5 \times 10^6$ for different initial conditions: (a) $l_3 = 0.2$, $l_5 = 0$, (b) $l_3 = 0$, $l_5 = 0$.

The far-field sound pressure levels (at the BPF of 262 Hz) were measured with a B&K microphone and the far-field noise spectra with and without control are shown in Fig. 11. The first harmonic reduced from 91 to 85 dB (relative to 20×10^{-6} Pa), the second harmonic reduced from 87 to 79 dB and the third harmonic increased from 77 to 82 dB.

5.3. Active control experiments at high speed

In the high-speed case there were three modes cut-on. The first control case had the first rod on the array acting as source and the second case had the first two rods as the source and the rest of the rods in each of these cases acting as controllers. The convergence of cost function (in-duct power in dB) in these cases is given in the two plots in Fig. 12. The cost function reduces in both cases, and the resulting level is considerably less variable than it was for the low-speed case, due to the increased sound levels relative to the background noise. The reduction of the in-duct noise power at BPF is around 2 dB in the two cases. The individual modal coupling coefficient variations for these cases are given in Figs. 13–15. Only modes $m = -1, 0$ reduce in amplitude; this should be expected because mode $m = 1$ cannot be controlled using the rods on the array when some of these rods are used as sources due to the in-phase contribution of each rod to this mode. Finally

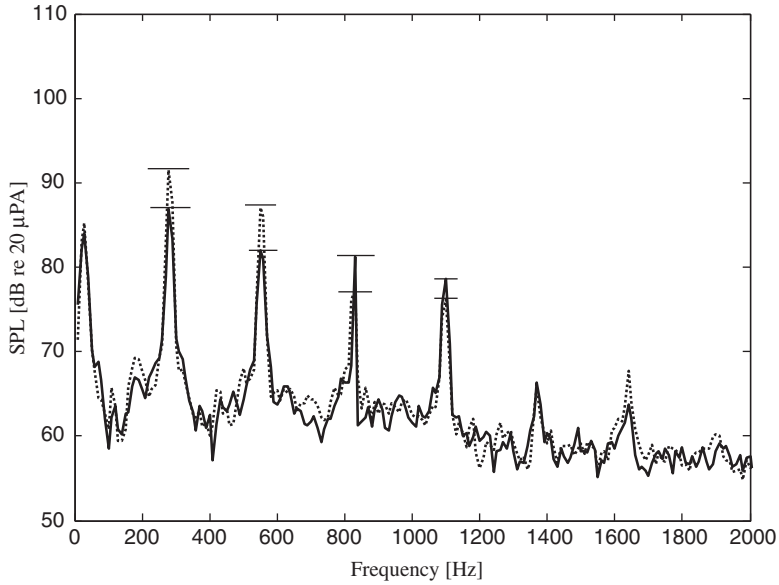

Fig. 11. Measured far-field noise spectra with and without control at low speed, BPF = 262 Hz.The primary field is generated by one source rod and two control rods have their lengths optimised to achieve the control. · · · · · without control, ——— with control. Horizontal lines show the levels of peaks.

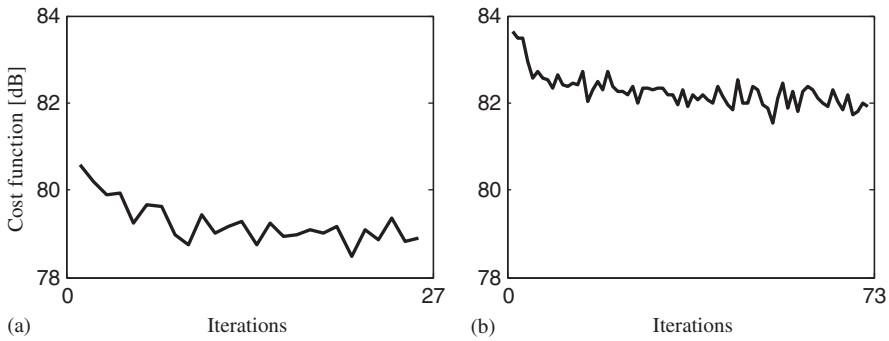

Fig. 12. Measured cost function time histories for control experiments at high speed with (a) one and (b) two rods used to generate the primary field. The convergence coefficient $\mu = 10^{5.}$.

the far-field noise spectra with and without control are shown in Fig. 16. As expected, the reduction at BPF (about 2 dB) is considerably less than that obtained at low speed for the reasons given above.

6. Conclusions

The simulations and experiments described above show that the steepest-descent algorithm is capable of adjusting control rods so as to reduce radiated noise, but that the attainable benefits depend on the relationship between the modal content and the number and position of the control rods. Future work might include an examination of a system with more modes present, including those with higher radial mode orders, and with quieter flow. The likely usefulness of a system such as the one described here will depend on its aerodynamic impact once optimised for this factor, and the relative importance of

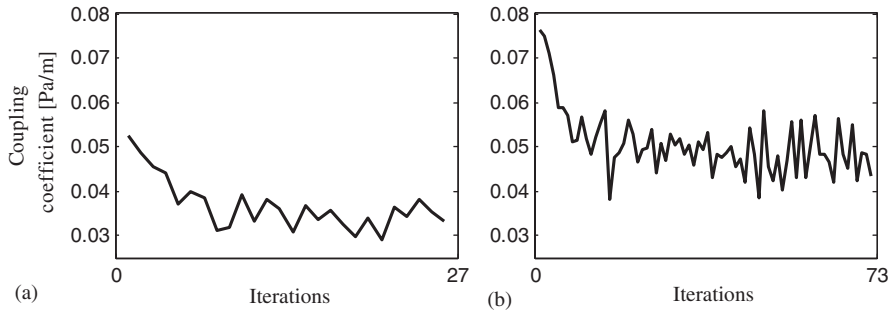

Fig. 13. Measured coupling coefficient time histories for mode $m = -1$ at high speed with (a) one and (b) two rods used to generate the primary field.

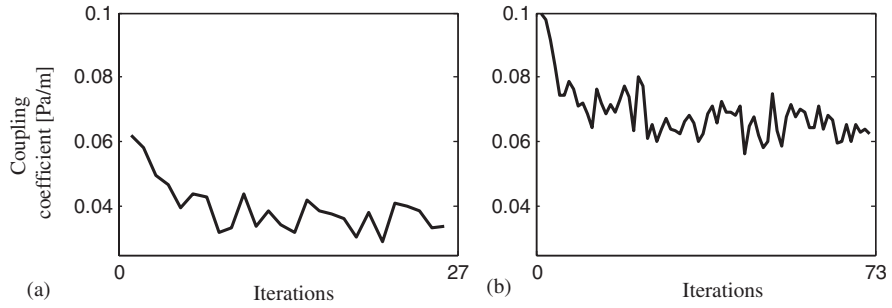

Fig. 14. Measured coupling coefficient variation for mode $m = 0$ at high speed with (a) one and (b) two rods used to generate the primary field.

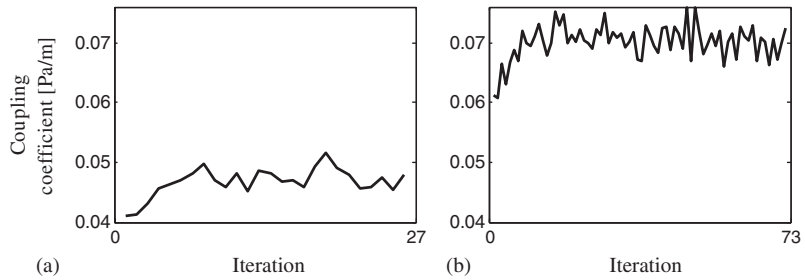

Fig. 15. Measured coupling coefficient variation for mode $m = 1$ at high speed with (a) one and (b) two rods used to generate the primary field.

aerodynamic and acoustic performance for the application in which it is employed. It must be borne in mind that any aerodynamic impact may require additional thrust, which may in turn generate higher noise generation, and this may be broadband as well as tonal. Future work may therefore have to look at the design of more advanced wake generators that can maximise their aeroacoustic effect over their aerodynamic effect.

One intriguing potential application area is in wind tunnel testing, where the presence of a model in the test area can cause distorted flow to impinge upon the tunnel fan and generate a distortion tone [23]. A system such as the one proposed here could be used to adaptively tune out the distortion tones caused by each different model that was placed in the tunnel, thus minimising expensive testing time.

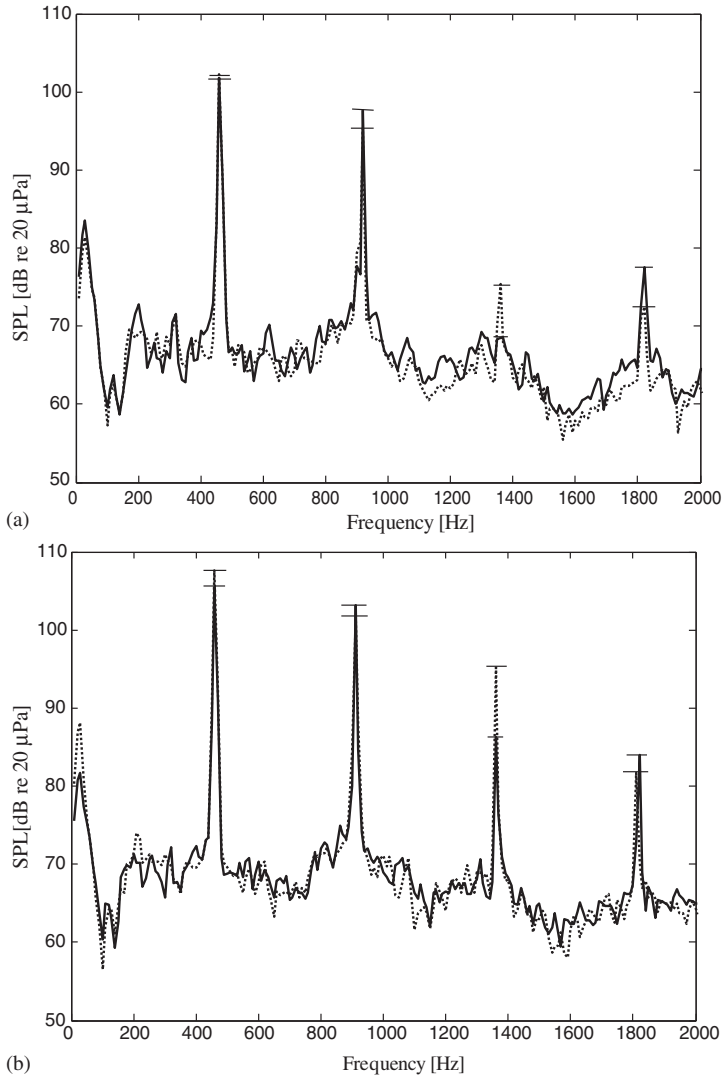

Fig. 16. Two examples of measured far-field noise spectra with and without control at high fan speed. The primary field is generated by (a) one and (b) two source rods and the remaining control rods have their lengths optimised to achieve the control. · · · · · without control, ———— with control. Horizontal lines show the levels of peaks.

Acknowledgements

This work was supported by the United Kingdom's Engineering and Physical Sciences Research Council Grant GR/M85296/01. It was originally suggested by P.A. Nelson.

References

[1] J.M. Tyler, T.G. Sofrin, Axial flow compressor noise studies, 1961, *SAE Transactions* 70 (1962) 309–332.
[2] M.E. Goldstein, *Aeroacoustics*, McGraw-Hill, New York, 1976.
[3] E. Envia, Fan noise reduction: an overview, *International Journal of Aeroacoustics* 1 (2002) 43–44.
[4] D.A. Topol, Rotor wake/stator interation noise: prediction vs. data, *Journal of Aircraft* 30 (1993) 728–735.
[5] R.P. Woodward, D.M. Elliott, C.E. Hughes, J.J. Berton, Benefits of swept and leaned stators for fan noise reduction, AIAA paper 99-0479, 1999.

[6] E. Envia, M. Nallasamy, Design selection and analysis of a swept and leaned stator concept, *Journal of Sound and Vibration* 228 (1999) 793–836.
[7] I.A. Waitz, J.M. Brookfield, J. Sell, B. Hayden, Preliminary assessment of wake management strategies for reduction of turbomachinery fan noise, *Journal of Propulsion and Power* 12 (1996) 958–966.
[8] D.L. Sutliff, D.L. Tweed, E.B. Fite, E. Envia, Low-speed fan noise reduction with trailing edge blowing, *International Journal of Aeroacoustics* 1 (2002) 275–305.
[9] G. Raman, D.K. McLaughlin (Eds.), *Highlights of Aeroacoustics Research in the US—1998*, AIAA paper 99-1915, 1999.
[10] C.J. Moore, Reduction of fan noise by annulus boundary layer removal, *Journal of Sound and Vibration* 43 (1975) 671–681.
[11] U. Ganz, S.A.L. Glegg, P. Joppa, Measurement and prediction of broadband fan noise, AIAA paper No. 98-2316, 1998.
[12] J.E. Ffowcs Williams, Noise, anti-noise and fluid flow control, *Philosophical Transactions of the Royal Society of London A* 360 (2002) 821–832.
[13] S. Sawyer, S. Fleeter, Active control of discrete-frequency noise generated by rotor–stator interactions, *Journal of Propulsion and Power* 18 (2002) 100–106.
[14] C. Polacsek, Reduction of fan rotor–stator interacting modes using a novel design: an experimental study, *Proceedings of the Sixth International Congress on Sound and Vibration* (ISCV), Copenhagen, 1999.
[15] C. Polacsek, F. Desbois-Lavergne, Fan interaction noise reduction using a wake generator: experiments and computational aeroacoustics, *Journal of Sound and Vibration* 265 (2003) 725–743.
[16] G. Fournier, J. Huard, J. Perucchini, Noise reduction of fans by control of flow distortion, *Internoise*, Yokohoma, 1994, pp. 519–522.
[17] P.A. Nelson, Active techniques and their potential for application in aeroacoustics, *Proceedings of the Sixth CEAS/AIAA Aeroacoustics Conference*, Lahaina, HI, 2000.
[18] C.L. Morfey, Sound transmission and generation in ducts with flow, *Journal of Sound and Vibration* 14 (1971) 37–55.
[19] C. Pitelet, Flow Control For Fan Noise Reduction, M.Sc. Thesis, University of Southampton, 2000.
[20] V. Kota, Wake Generator Control of Flow Distortion Induced Tonal Noise in Fans, PhD Thesis, University of Southampton, 2005.
[21] P.E. Gill, W. Murray, M.H. Wright, *Practical Optimization*, Academic Press, San Diego, 1981.
[22] BS EN ISO 5136, Acoustics: determination of sound power radiated into a duct by fans and other air-moving devices—in-duct method, 2003.
[23] T.J. Mueller, D.A. Lynch, An anechoic facility for basic aeroacoustic research, in: T.J. Mueller (Ed.), *Aeroacoustic Measurement*, Springer, Berlin, 2002, pp. 283–304.